laboratory notes

Development of a simultaneous measurement system for SAXS–WAXD and the thickness of coating films during film formation by solvent evaporation

Keisuke Shimokita,[a] Tsukasa Miyazaki,[a]* Hiroki Ogawa[b] and Katsuhiro Yamamoto[c]

[a]Functional Design Technology Center, Nitto Denko Corporation, Shimohozumi, Ibaraki, Osaka, 567-8680, Japan, [b]Japan Synchrotron Radiation Research Institute, Kouto, Sayo, Hyogo, 679-5198, Japan, and [c]Department of Materials Science, Nagoya Institute of Technology, Gokiso-cho, Showa-ku, Nagoya, 466-8555, Japan. Correspondence e-mail: tsukasa_miyazaki@gg.nitto.co.jp

A system for the simultaneous measurement of small-angle X-ray scattering and wide-angle X-ray diffraction (SAXS–WAXD) and the thickness of a coating film, obtained with an automatic coater, during film formation has been developed. The system was installed on beamline BL03XU at SPring-8. As model specimens, poly(methyl methacrylate)-*b*-poly(*n*-butyl acrylate)-*b*-poly-(methyl methacrylate) (PMMA-*b*-PnBA-*b*-PMMA) triblock copolymers with different compositions were used to investigate the film formation process during solvent evaporation. First of all, the data correction methods were examined for the coating films during solvent evaporation. Since the scattering invariant was affected by the scattering volume and the absorption of X-rays by the solvent and the copolymer during drying, the scattering invariant should be corrected for the film width and the X-ray absorption of the sample. The polymer concentration was estimated from the thickness of the coating film during solvent evaporation, while the X-ray absorption was evaluated by using the X-ray linear absorption coefficients of the solvent and the copolymer. The results showed that the correction of the scattering invariant is crucial for an exact description of the film formation process during solvent evaporation.

1. Introduction

Commercially available polymer films have been widely used in various industrial applications, such as optical films, membranes, adhesive tapes and so on (Miyazaki *et al.*, 2007; Schmidegg *et al.*, 2006; Khayet *et al.*, 2002; Liu *et al.*, 2013; Townsend *et al.*, 2011). The film properties depend substantially on the film formation processes, because polymer structures in the film may be dramatically changed by the processing conditions. In particular, it is well known that polymer films produced by solvent evaporation methods have a so-called skin layer, which is generally denser than the bulk, at the air–solution interface during their formation process (Ghoshal *et al.*, 2012; Ciampi & McDonald, 2003). The formation of the skin layer probably leads to different structures in the polymer film because it slows down the solvent evaporation rate.

For thin films with a thickness within a range of several hundreds of nanometres, it is suggested that the film structures and properties differ considerably from those of thick films (Miyazaki *et al.*, 2004; Jin *et al.*, 2007; Tolan *et al.*, 2000; Keddie *et al.*, 1994). However, for films prepared with thin-film formation methods that rely on solvent evaporation, such as casting, dip coating and spin coating, a number of complex interactions are still present in the surface and film–substrate interface regions, making it difficult to understand the difference in nature between the thin film and the bulk polymer (Kim *et al.*, 2002; Ho *et al.*, 2005; Liang *et al.*, 2007; Thomas *et al.*, 2010). In addition to mobile surface layers with lower glass transition

temperatures, an immobile rigid layer involving oriented molecules attributed to film–substrate interactions may be produced at the film–substrate interface (Park *et al.*, 2009; Kao *et al.*, 2011; Fukunaga *et al.*, 2003; Grohens *et al.*, 1998). There are a lot of experiments in which the film–substrate interaction is utilized in order to control the polymer ordering (Park *et al.*, 2009; Lösche *et al.*, 1998; Despoto-poulou *et al.*, 1996).

Characterizing and controlling the structure of the heterogeneous layers at surfaces and interfaces are key factors for applications to industrial products. The polymer structures present after film formation under various processing conditions have been examined, so far, by various methods such as transmission electron microscopy, atomic force microscopy, small-angle X-ray scattering (SAXS) and wide-angle X-ray diffraction (WAXD) (Niihara *et al.*, 2007, 2008; Yakabe *et al.*, 2003; Park *et al.*, 2007; Li *et al.*, 2001). However, it is important to observe the film formation processes *in situ* during solvent evaporation in order to clarify the film formation mechanism. Nevertheless, only a few experiments have been conducted on the formation of films during solvent evaporation (Heinzer *et al.*, 2012*a,b*; Gong *et al.*, 2006; Kim & Libera, 1998).

Therefore, we have constructed a simultaneous SAXS–WAXD and film thickness measurement system with an automatic coater. Synchrotron X-rays are used because incident beams with a high flux intensity allow structural information to be obtained *in situ*, and spectral interferometry is used to monitor the thickness of the coating film. Thus, a simultaneous examination of the structure and the

polymer concentration in solution and the solvent evaporation rate during film formation can be carried out.

In this note, we describe first the home-made coater constructed for simultaneous SAXS–WAXD and film thickness measurements during solvent evaporation. Secondly, the correction of the X-ray scattering invariant under solvent removal is discussed. Finally, we show the preliminary results obtained on the drying process of triblock copolymer solutions by using the newly developed coater.
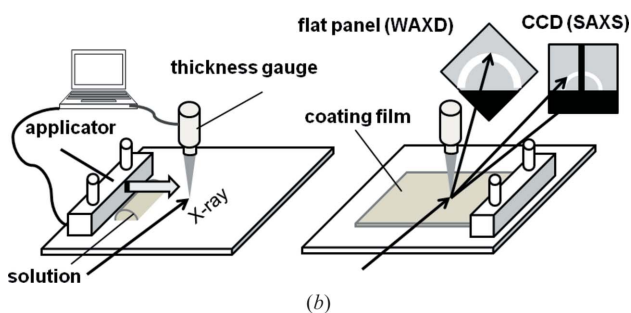
2. Simultaneous SAXS–WAXD and film thickness measurement system with an automatic coater

Simultaneous SAXS–WAXD and film thickness measurements were performed on beamline BL03XU at SPring-8. The basic beamline configuration is described elsewhere (Masunaga *et al.*, 2011; Ogawa *et al.*, 2013).

We developed an automatic coater (Fig. 1a) using applicators with various clearances to investigate the structural development in polymer solutions *in situ* during film formation by solvent evaporation. It was directly located on the height stage of the diffractometer in the first experimental hutch of BL03XU (Ogawa *et al.*, 2013). The first hutch was designed for grazing-incidence WAXD and SAXS experiments, with the diffractometer allowing a specimen to be set accurately into the incident X-ray beam. The incident X-ray beam is easily aligned to irradiate the coating films in the film thickness direction. The area of the coating stage is 90×90 mm. Si wafers with a thickness of 625 µm were used as the substrates. The coating stage is
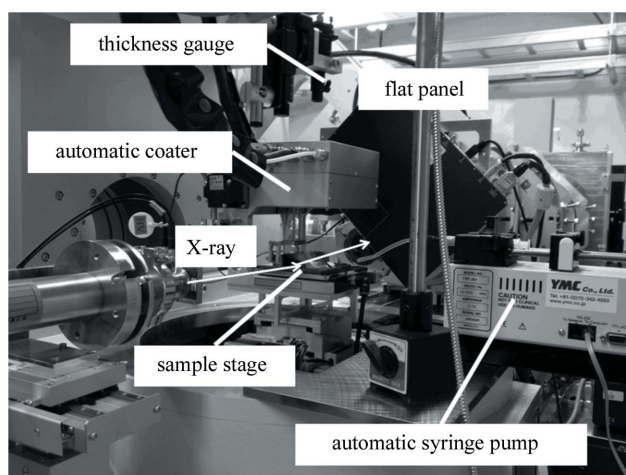
(a)

(b)

Figure 1
(a) The home-made automatic coater equipped on the height stage of BL03XU at SPring-8. A film thickness gauge and an automatic syringe pump are also set up. (b) An illustration of the simultaneous measurement system of SAXS–WAXD and film thickness.

equipped with four cartridge heaters (4×90 W), allowing coating solutions to be dried at temperatures up to 473 K. The final film thickness can be controlled by the clearance between the applicator and the substrate and by the initial solution concentration. The clearance is selected within a range of 20–250 µm. Since the coating direction is remotely switched from the left side to the right side and the coater is mounted on a rotary stage, the X-ray beam enters the end or edge direction of the coating film. The applicator holder is equipped with air cylinders. Therefore, the applicator automatically rises above 40 mm after coating, allowing X-ray scattering measurements with a diffraction angle in the range up to 45° for WAXD.

A film thickness gauge (Hamamatsu Photonics, Optical Nano-Gauge C10178-01S) is set up in order to monitor the coating film thickness during solvent evaporation, and the probe head of the thickness gauge is mounted above the coater, as shown in Fig. 1(a). The film thickness was measured *in situ* by using a white light spectroscopic reflectometer, which analyzes multiple reflections between the air–film and the film–substrate interfaces when white light is irradiated into the coating film. The working distance of the thickness gauge is around 230 mm and the measurement area is about 10 mm in diameter. The probe head is connected to the spectroscope *via* an optical fiber, which is controlled by a dedicated software program on a laptop. The minimum measurement interval is 19 ms, which makes tracking of the thickness possible even if very fast solvent evaporation occurs. In this work, the measurement interval is 1 s.

For the SAXS–WAXD experiment, the X-ray wavelength was tuned at 0.1 nm and the beam size at the sample position was 200×100 µm (horizontal $\times$ vertical). The sample-to-detector distances were 1876 and 171 mm for SAXS and WAXD, respectively. Two-dimensional images for SAXS were collected on a cooled CCD (Hamamatsu Photonics, V7739P+ORCA R2) consisting of 1344×1024 pixels (pixel size 63 µm^2) with an X-ray image intensifier and for WAXD on a flat-panel detector (Hamamatsu Photonics, C9827DK-10) consisting of 1024×1024 pixels (pixel size 50 µm^2). The exposure time of the CCD detector was 500 ms.

Experimental procedures are schematically indicated in Fig. 1(b). An ~0.2 ml solution of the coating material was deposited onto the substrate by an automatic syringe pump and then spread on the substrate with an applicator in a direction perpendicular to the incident X-ray direction. Simultaneous measurements of SAXS–WAXD and the film thickness are performed immediately after coating. In this work, the incident angle of the X-ray beam was fixed at 0°, which is the angle between the incident beam and the sample surface, although the setup makes grazing-incidence X-ray scattering measurements possible for very thin films.

3. Correction of X-ray scattering invariant

As model specimens, we used two kinds of poly(methyl methacrylate)-*b*-poly(*n*-butyl acrylate)-*b*-poly(methyl methacrylate) (PMMA-*b*-PnBA-*b*-PMMA) triblock copolymers (LA2250 and LA4285), which have different compositions (LA2250: $M_w = 5.8 \times 10^4$, $M_w/M_n = 1.19$, weight fraction of PnBA = 70 wt%; LA4285: $M_w = 5.8 \times 10^4$, $M_w/M_n = 1.11$, weight fraction of PnBA = 50 wt%). They were purchased from Kuraray Co. Ltd. Toluene, which was purchased from Wako Pure Chemical Industries Ltd, was used to dissolve both triblock copolymers. All materials were used without any purification. The solutions were stirred at room temperature for 24 h and then left at room temperature for a further 24 h to remove bubbles. For the two coating solutions the initial polymer concentration was 25.2 vol.%. Microphase separations occur during solvent evaporation

laboratory notes

on film formation for these triblock copolymers, so it is crucial to examine the scattering invariant in order to study the structural formation of the polymers. Firstly, the X-ray scattering invariant is normalized by the scattering volume. Secondly, a correction for X-ray absorption by the sample during solvent evaporation is required. This is because the width of the coating films is several centimetres in our case, which is too large for an examination of the scattered X-rays without an absorption correction. It is likely that the X-ray absorption varies as a function of time or the polymer concentration during solvent evaporation since the polymer fraction in the solution changes.

As a result, we correct the X-ray scattering invariant, P, by using the following equation:

$$P = \frac{\int I(q)\, q^2\, dq}{twC_{\text{poly}} \exp(-\mu_{\text{sol}}w)}, \tag{1}$$

where q is the modulus of the scattering vector, $I(q)$ is the X-ray scattering intensity, t is the coating film thickness, w is the width of the coating film through which the X-rays pass, C_{poly} is the polymer concentration and μ_{sol} is the X-ray linear absorption coefficient of the solution. q is calculated from the corresponding scattering angle (2θ):

$$q = (4\pi/\lambda)\sin\theta. \tag{2}$$

Here, λ is the wavelength of the X-ray beam. q_y and q_z are the scattering vector components parallel and normal to the substrate, respectively.

It should be noted that the coating film thickness measured during film formation is within the vertical beam size of 100 µm. In addition to the film thickness and the width, we have to obtain the polymer concentration, C_{poly}, in the solution and the X-ray linear absorption coefficient of the solution, μ_{sol}, to correct the invariant by equation (1) during film formation. However, by using equation (3), we can

calculate the polymer concentration from the coating film thickness, assuming that the polymer volume and the coating film width do not change during the solvent removal:

$$C_{\text{poly}} = (t^0 C_{\text{poly}}^0)/t, \tag{3}$$

where t and t^0 are the film thickness at an arbitrary time and the initial time, respectively. C_{poly}^0 is the initial polymer concentration. Equation (3) indicates that $C_{\text{poly}}t$ is constant during evaporation. Therefore, equation (1) can be converted into the simple expression

$$P = \frac{\int I(q)\, q^2\, dq}{w \exp(-\mu_{\text{sol}}w)}. \tag{4}$$

For example, in the case of the LA2250 solution with a polymer concentration of 25.2 vol.% as a coating solution, we calculated the polymer concentration with the thickness of the coating film during solvent evaporation. Fig. 2(a) shows how the coating film thickness changes as toluene evaporates. The film thickness is 55 µm just after coating and it decreases at a rate of 0.35 µm s^{-1} for 100 s. Then, the rate of decrease reduces with time and is nearly 0 µm s^{-1} at 250 s, which implies that the toluene has almost completely evaporated from the coating film.

Fig. 2(b) shows the changes in polymer concentration as a function of time.

Next, the X-ray linear absorption coefficients of the solutions with various polymer concentrations should be obtained in order to correct the X-ray absorption of the solutions. The X-ray transmittances of the solutions in cells with widths of 3, 5, 7, 10 and 15 mm were measured. Solutions of LA2250–toluene with polymer concentrations of 0.0, 4.0, 8.1, 16.5 and 25.2 vol.% were put into the cells. The X-ray transmittances of the solutions can be estimated with an ion chamber. Fig. 3(a) shows the cell width dependence of the transmittance of each polymer solution. From these data we can
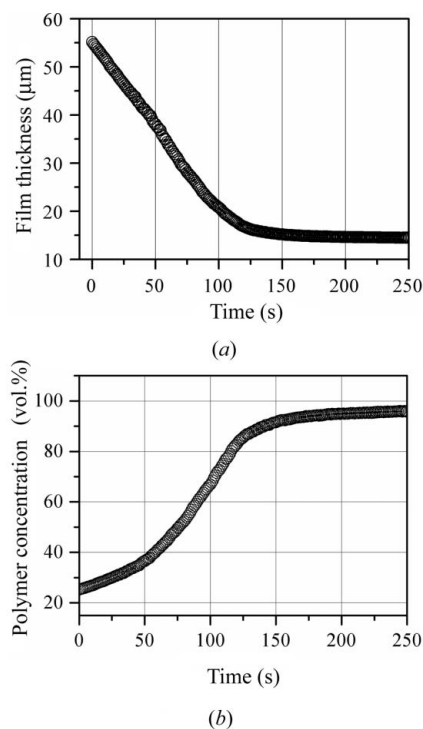
Figure 2
(a) The thickness variation of the coating film of an LA2250 solution at room temperature as a function of time. (b) The polymer concentration calculated from the thickness variation in (a).
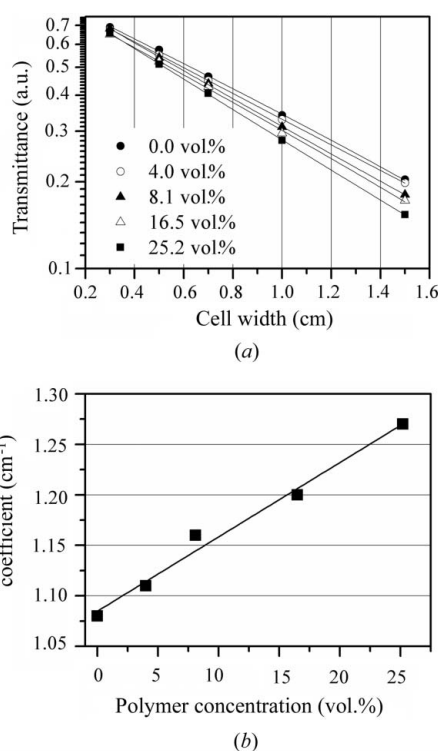
Figure 3
(a) The correlation between the X-ray transmittance and the cell width in the LA2250 solutions at various polymer concentrations. (b) The X-ray linear absorption coefficients *versus* the polymer concentrations in the LA2250 solutions.

Table 1
Linear absorption coefficients of the LA2250 solutions in various polymer concentrations.

Polymer concentration (vol.%)	Measured coefficient (cm^{-1})	Calculated coefficient (cm^{-1})
0.0	1.08	0.99
4.0	1.11	1.02
8.1	1.16	1.05
16.5	1.20	1.12
25.2	1.27	1.19
100.0	1.81	1.77

determine the linear dependence of the X-ray linear absorption coefficients of the solutions on the polymer concentration, as shown in Fig. 3(b) and summarized in Table 1, which includes data for the 100 vol.% polymer. This enables us to obtain X-ray linear absorption coefficients for the solution concentrations by interpolation.

In addition, X-ray linear absorption coefficients can be calculated from data given by Sasaki (1990). The X-ray linear absorption coefficients of the solutions calculated with various polymer concentrations using Sasaki's data are presented in Table 1.

The X-ray linear absorption coefficients increase with increasing polymer concentration. The calculated values are in agreement with those measured for each solution within 15%, although the calculated ones may be underestimated (Sasaki, 1990). It is confirmed that the X-ray linear absorption coefficients are substantially changeable depending on the polymer concentration. Therefore, it is certainly important to correct the X-ray scattering invariant for changes in X-ray absorption during the coating film formation process. As indicated above, the good agreement between the X-ray linear absorption coefficients obtained experimentally and those calculated on the basis of Sasaki's data suggests that the calculated values are generally applicable to the various coating films composed of different polymers and solutions.

4. Preliminary results

Simultaneous SAXS–WAXD and film thickness measurements were performed for solutions of both LA2250 and LA4285 during film formation. The two-dimensional SAXS patterns obtained during drying were analyzed for the determination of the scattering invariants and the correlation lengths in the directions normal, d_z, and parallel, d_y, to the film surface. d_z and d_y are obtained with the scattering peak positions in the normal and the horizontal directions by using Bragg's law, $d = 2\pi/q$. Figs. 4(a) and 4(b) indicate d_z, d_y and the scattering invariant corrected with equation (4) during film formation for the LA2250 and the LA4285 solutions, respectively. Selected two-dimensional X-ray scattering patterns for LA2250 solutions of 25.2, 31.1, 37.2, 53.7, 82.8 and 95.1 vol.% and for LA4285 solutions of 25.2, 27.2, 36.0, 52.9, 74.1 and 90.5 vol.% are also shown.

It is found that the microphase separations in both the LA2250 and the LA4285 solutions do not occur immediately after coating. However, isotropic scattering patterns which are caused by microphase separations between PnBA phases and PMMA phases can be observed above 31.1 vol.% in the LA2250 solutions and 27.2 vol.% in the LA4285 solutions.

d_y is almost constant during solvent evaporation for both solutions, which probably shows that the coating film is pinned on the substrate in the horizontal direction (Heinzer et al., 2012a,b). While d_z is constant until 60 vol.% in both the LA2250 and the LA4285 solutions, after that it decreases with increasing polymer concentration up to 83 vol.% in the LA2250 solutions and 89 vol.% in the LA4285

solutions and then becomes constant again. These results suggest that these coating films are compressed in the vertical direction in accordance with the shrinkage of the films owing to deswelling of the ordered domains, while they have the same ordered space in the horizontal direction with the pinning on the substrate during solvent
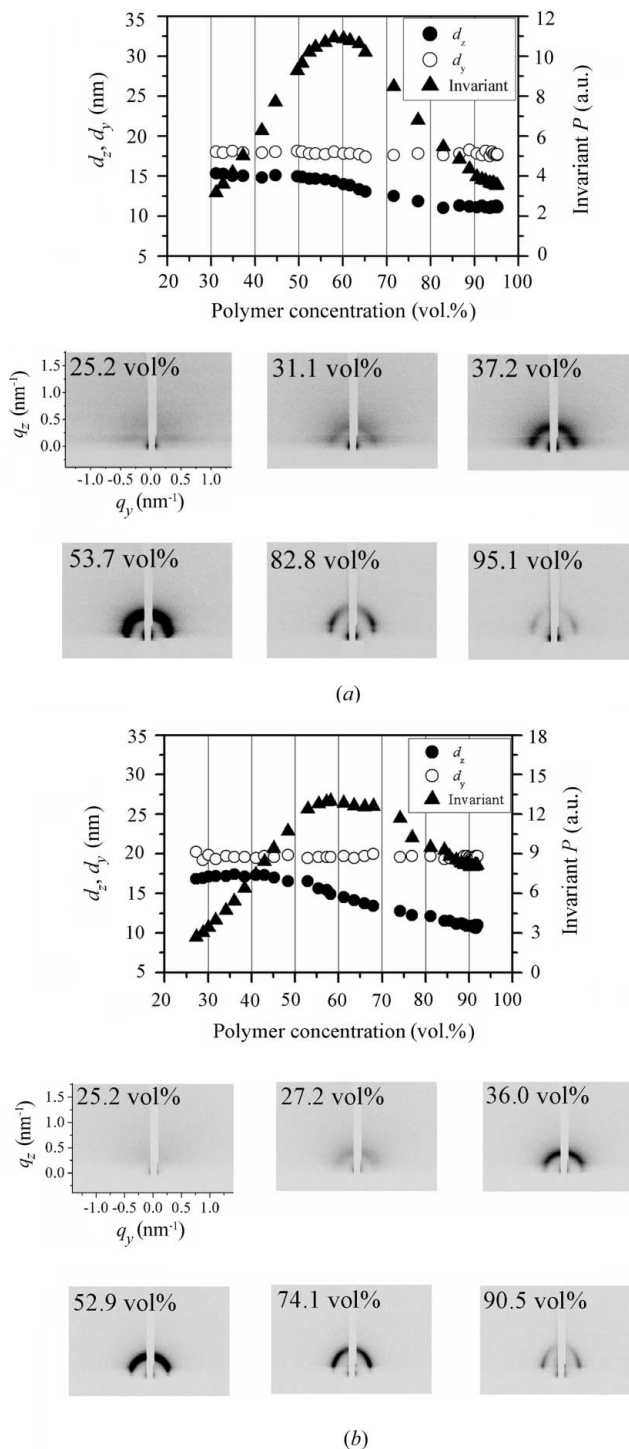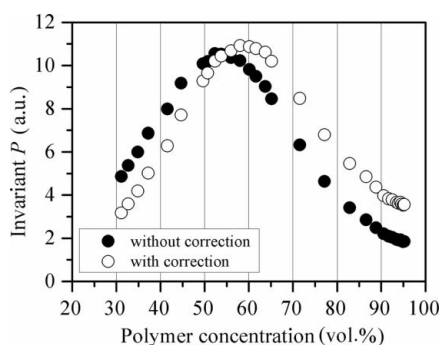

Figure 4
Correlation lengths in the directions normal, d_z (filled circles), and parallel, d_y (open circles), to the film surface obtained by using Bragg's law and the scattering invariant, P (filled triangles), as a function of polymer concentration (a) for the LA2250 solutions and (b) for the LA4285 solutions. Selected two-dimensional X-ray scattering patterns are also presented in (a) for the LA2250 solutions and in (b) for the LA4285 solutions at various polymer concentrations.

evaporation. Similar results were shown using poly(styrene-*b*-butadiene) block copolymer (Heinzer *et al.*, 2012*a,b*).

The scattering invariant also increases rapidly with increasing polymer concentration up to 60 vol.% in both the LA2250 and the LA4285 solutions, and then it starts to decrease until the solvent is almost evaporated from the film. In addition to the development of the microphase separation, the substantial increase in the scattering invariant suggests that the preferential evaporation of the solvent from either the PnBA or the PMMA phases enlarges the electron density difference between the PnBA and the PMMA phases in the early stage of evaporation. The Flory-Huggins interaction parameters of PMMA and PnBA to toluene are about 0.5 and 0.1 at room temperature, respectively (Brandrup *et al.*, 1999), leading to preferential toluene evaporation from PMMA phases prior to that from PnBA phases. As a result, the preferential evaporation from PMMA phases enhances the scattering invariant in the early stage of microphase separation as well as its development. On the other hand, beyond 60 vol.% in both the LA2250 and the LA4285 solutions, the toluene that remained in the film evaporates mainly from the PnBA phases, resulting in a small density difference which leads to a decrease in the scattering invariant. As shown in Fig. 4, the decreases in the scattering invariant and d_z take place simultaneously. This must also indicate that toluene evaporation from the PnBA phases causes the predominant decrease in d_z, because it is suggested that toluene evaporation from the backbone structures composed of PnBA phases shrinks the film in the film thickness direction.

As described above, the correction of the scattering invariant is necessary for the investigation of the relationship between the change in the scattering invariant and the correlation length. Fig. 5 shows the change in the scattering invariant with and without the correction for the LA2250 solutions as indicated in Fig. 4(*a*). The peak position and the trend of the scattering invariant variation with the correction are different from those without the correction. When the correction is performed, the polymer concentration corresponding to the peak position in the curve in Fig. 5 is the same as the concentration at the onset of the decrease in q_z, suggesting that the occurrence of the film shrinkage corresponds to the onset of the preferential solvent evaporation, as described above. On the other hand, the peak position in the scattering invariant curve is not in agreement with the concentration at the onset of the shrinkage of the backbone structure when the scattering invariant is not corrected. Although further detailed investigation is required for declaring the origin of the change in the scattering invariant and the decrease in d_z, it is important to take this correction into consideration when discussing the structural changes in a polymer during solvent evaporation.

In conclusion, we succeeded in constructing a system for simultaneous measurement of SAXS–WAXD and the thickness of a coating film and in accurately correcting the scattering invariant for the film during solvent evaporation. We will use the system to investigate the structural formation mechanisms for various polymer–solvent systems, including block copolymer solutions, for which the results are preliminarily indicated in this note, and semicrystalline polymer solutions relating to the kinetics of crystallization during solvent evaporation.

In particular, the skin layer must be formed in the early stage of the film formation process. In fact, for the LA2250 solutions in this note the very weak in-plane-oriented scattering seems to appear prior to the occurrence of the isotropic scattering attributed to a disordered microphase separation in the bulk, probably suggesting the formation of a skin layer at the surface region in the early stage of evaporation. We will investigate the effects of the evaporation conditions, such as the evaporation temperature and the evaporation atmosphere, on the skin layer formation in the future. As mentioned in the *Introduction*, heterogeneous structural formation in film–substrate interface regions should be investigated as well as in surface regions.

References

Brandrup, J., Immergut, E. H. & Grulke, E. A. (1999). *Polymer Handbook*, 4th ed., pp. 247–264. New York: John Wiley and Sons.
Ciampi, E. & McDonald, P. J. (2003). *Macromolecules*, **36**, 8398–8405.
Despotopoulou, M. M., Miller, R. D., Rabolt, J. F. & Frank, C. W. (1996). *J. Polym. Sci. Polym. Phys.* **34**, 2335–2349.
Fukunaga, K., Hashimoto, T., Elbs, H. & Krausch, G. (2003). *Macromolecules*, **36**, 2852–2861.
Ghoshal, S., Denner, P., Stapf, S. & Mattea, C. (2012). *Macromolecules*, **45**, 1913–1923.
Gong, Y., Huang, H., Hu, Z., Chen, Y., Chen, D., Wang, Z. & He, T. (2006). *Macromolecules*, **39**, 3369–3376.
Grohens, Y., Brogly, M., Labbe, C., David, M. & Schultz, J. (1998). *Langmuir*, **14**, 2929–2932.
Heinzer, M. J., Han, S., Pople, J. A., Baird, D. G. & Martin, S. M. (2012*a*). *Macromolecules*, **45**, 3471–3479.
Heinzer, M. J., Han, S., Pople, J. A., Baird, D. G. & Martin, S. M. (2012*b*). *Macromolecules*, **45**, 3480–3486.
Ho, R., Tseng, W., Fan, H., Chiang, Y., Lin, C., Ko, B. & Huang, B. (2005). *Polymer*, **46**, 9362–9377.
Jin, S., Yoon, J., Heo, K., Park, H.-W., Kim, J., Kim, K.-W., Shin, T. J., Chang, T. & Ree, M. (2007). *J. Appl. Cryst.* **40**, 950–958.
Kao, J., Tingsanchali, J. & Xu, T. (2011). *Macromolecules*, **44**, 4392–4400.
Keddie, J. L., Jones, R. A. L. & Cory, R. A. (1994). *Europhys. Lett.* **27**, 59–64.
Khayet, M., Feng, C. Y., Khulbe, K. C. & Matsuura, T. (2002). *Polymer*, **43**, 3879–3890.
Kim, G. & Libera, M. (1998). *Macromolecules*, **31**, 2569–2577.
Kim, S. H., Misner, M. J., Xu, T., Kimura, M. & Russell, T. P. (2002). *Adv. Mater.* **14**, 226–231.
Li, L., Chan, C., Yeung, K. L., Li, J., Ng, K. & Lei, Y. (2001). *Macromolecules*, **34**, 316–325.
Liang, G. D., Xu, J. T. & Fan, Z. Q. (2007). *J. Phys. Chem. B*, **111**, 11921–11928.
Liu, Y., Wang, R., Ma, H., Hsiao, B. S. & Chu, B. (2013). *Polymer*, **54**, 548–556.
Lösche, M., Schmitt, J., Decher, G., Bouwman, W. G. & Kjaer, K. (1998). *Macromolecules*, **31**, 8893–8906.
Masunaga, H. *et al.* (2011). *Polym. J.* **43**, 471–477.
Miyazaki, T., Hoshiko, A., Akasaka, M., Sakai, M., Takeda, Y. & Sakurai, S. (2007). *Macromolecules*, **40**, 8277–8284.

Figure 5
Scattering invariants obtained by SAXS measurements for the LA2250 solutions with and without correction.

Miyazaki, T., Nishida, K. & Kanaya, T. (2004). *Phys. Rev. E*, **69**, 061803.

Niihara, K., Matsuwaki, U., Torikai, N., Atarashi, H., Tanaka, K. & Jinnai, H. (2007). *Macromolecules*, **40**, 6940–6946.

Niihara, K., Sugimori, H., Matsuwaki, U., Hirato, F., Morita, H., Doi, M., Masunaga, H., Sasaki, S. & Jinnai, H. (2008). *Macromolecules*, **41**, 9318–9325.

Ogawa, H. *et al.* (2013). *Polym. J.* **45**, 109–116.

Park, H., Im, K., Chung, B., Ree, M., Chang, T., Sawa, K. & Jinnai, H. (2007). *Macromolecules*, **40**, 2603–2605.

Park, S., Lee, D. H., Xu, J., Kim, B., Hong, S. W., Jeong, U., Xu, T. & Russell, T. P. (2009). *Science*, **20**, 1030–1033.

Sasaki, S. (1990). *KEK Rep.* **90-16**, 1–143.

Schmidegg, K., Sun, L., Maier, G., Keckes, J. & Zeppenfeld, P. (2006). *Polymer*, **47**, 4768–4772.

Thomas, K. R., Clarke, N., Poetes, R., Morariu, M. & Steiner, U. (2010). *Soft Matter*, **6**, 3517.

Tolan, M., Seeck, O. H., Wang, J., Sinha, S. K., Rafailovich, M. H. & Sokolov, J. (2000). *Physica B*, **283**, 22–26.

Townsend, B. W., Ohanehi, D. C., Dillard, D. A., Austin, S. R., Salmon, F. & Gagnon, D. R. (2011). *Int. J. Adhes. Adhes.* **31**, 650–659.

Yakabe, H., Sasaki, S., Sakata, O., Takahara, A. & Kajiyama, T. (2003). *Macromolecules*, **36**, 5905–5907.